

NANO EXPRESS

Open Access

Impact of device size and thickness of Al_2O_3 film on the Cu pillar and resistive switching characteristics for 3D cross-point memory application

Rajeswar Panja, Sourav Roy, Debanjan Jana and Siddheswar Maikap*

Abstract

Impact of the device size and thickness of Al_2O_3 film on the Cu pillars and resistive switching memory characteristics of the $\text{Al}/\text{Cu}/\text{Al}_2\text{O}_3/\text{TiN}$ structures have been investigated for the first time. The memory device size and thickness of Al_2O_3 of 18 nm are observed by transmission electron microscope image. The 20-nm-thick Al_2O_3 films have been used for the Cu pillar formation (i.e., stronger Cu filaments) in the $\text{Al}/\text{Cu}/\text{Al}_2\text{O}_3/\text{TiN}$ structures, which can be used for three-dimensional (3D) cross-point architecture as reported previously *Nanoscale Res. Lett.* 9:366, 2014. Fifty randomly picked devices with sizes ranging from 8×8 to $0.4 \times 0.4 \mu\text{m}^2$ have been measured. The $8\text{-}\mu\text{m}$ devices show 100% yield of Cu pillars, whereas only 74% successful is observed for the $0.4\text{-}\mu\text{m}$ devices, because smaller size devices have higher Joule heating effect and larger size devices show long read endurance of 10^5 cycles at a high read voltage of -1.5 V. On the other hand, the resistive switching memory characteristics of the $0.4\text{-}\mu\text{m}$ devices with a 2-nm-thick Al_2O_3 film show superior as compared to those of both the larger device sizes and thicker (10 nm) Al_2O_3 film, owing to higher Cu diffusion rate for the larger size and thicker Al_2O_3 film. In consequence, higher device-to-device uniformity of 88% and lower average RESET current of approximately $328 \mu\text{A}$ are observed for the $0.4\text{-}\mu\text{m}$ devices with a 2-nm-thick Al_2O_3 film. Data retention capability of our memory device of >48 h makes it a promising one for future nanoscale nonvolatile application. This conductive bridging resistive random access memory (CBRAM) device is forming free at a current compliance (CC) of $30 \mu\text{A}$ (even at a lowest CC of $0.1 \mu\text{A}$) and operation voltage of ± 3 V at a high resistance ratio of $>10^4$.

Keywords: Resistive switching; Al_2O_3 ; Cu pillar; 3D memory; CBRAM

Background

It is known that commercial FLASH memory approaches its scaling limit in sub-20-nm technology node. As it is an alternative solution to replace the FLASH, resistive random access memory (RRAM) becomes a center of attraction to the researchers because of its simple metal-insulator-metal (MIM) structure with low voltage operation (<3 V), high speed operation, and high scalability potential (<10 nm) [1-5]. Although many switching materials have been reported for the RRAM applications, the Al_2O_3 as a switching material has been reported a few [6-9]. The amorphous Al_2O_3 film has energy gap of 6.2 to 8.8 eV [10,11], dielectric constant of 9 [12], and

Gibbs free energy of $-1,582.3$ kJ/mole at 300 K [13], which can help to have good resistive switching properties. Wu et al. [6] have described a $\text{TiN}/\text{Al}_2\text{O}_3/\text{Pt}$ RRAM device with a current compliance (CC) of sub- $20 \mu\text{A}$ and high operating voltage of $+8/-4$ V. Wu et al. [14] have reported the $\text{Al}/\text{Al}_2\text{O}_3/\text{Pt}$ RRAM devices with an unstable RESET current of $1 \mu\text{A}$. Lin et al. [7] have reported the resistive switching characteristics using a $\text{Ti}/\text{Al}_2\text{O}_3/\text{Pt}$ structure with a high CC of 10 mA and operating voltage of ± 3 V. We have reported the resistive switching memory characteristics using an $\text{IrO}_x/\text{Al}_2\text{O}_3/\text{IrO}_x\text{-NDs}/\text{Al}_2\text{O}_3/\text{W}$ structure with a CC/voltage of $500 \mu\text{A}/\pm 4$ V previously [8]. The resistive switching phenomena using an $\text{IrO}_x/\text{AlO}_x/\text{W}$ structure with a CC of $200 \mu\text{A}$ in cross-point architecture have been also reported by us [9]. In this regard, many chalcogenide materials in the conductive bridging resistive

* Correspondence: sidhu@mail.cgu.edu.tw

Thin Film Nano Tech. Lab., Department of Electronic Engineering, Chang Gung University, 259 Wen-Hua 1st Rd., Kwei-Shan, Tao-Yuan 333, Taiwan

random access memory (CBRAM) devices have also been reported by many groups [15–23]. Basically, silver (Ag) or Cu is used as an oxidizing electrode, and the metal ions are migrated through the chalcogenide material under a positive bias on the Ag or Cu electrode. Recently, the AlO_x material in the CBRAM devices using the Ag (or Cu)/ Al_2O_3 /bottom electrode (BE) structures [24–26] has emerged great interest to the researchers due to its high compatibility with the fabrication of conventional CMOS devices. Goux et al. [24] have reported the CBRAM devices using a Cu-Te/ Al_2O_3 /Si structure at a CC of 5 μA and operating voltage of +0.5/–1 V. In this case, they have used a thin layer (approximately 3 nm) of Al_2O_3 film as an active material and device size was large $1 \times 1 \text{ mm}^2$. Sleiman et al. [25] have investigated the Cu/ AlO_x /W CBRAM devices with a CC of 100 μA and operating voltage of ± 2 V. The thickness of AlO_x layer is 20 nm, and a large device size is $1 \times 1 \text{ mm}^2$. Belmonte et al. [26] have described the resistive switching characteristics in 90-nm Cu/TiW/ Al_2O_3 /W 1T1R integrated cell, and they have introduced the TiW as a buffer layer to protect Cu diffusion. In this case, the thickness of Al_2O_3 layer is 3 nm. The memory device could be operated at 25 μA with operation voltage of ± 2 V. It is noticed that the Al_2O_3 material has been used in the CBRAM devices using bi-layers and different structures and thicknesses. However, impact of device size and thickness of a single Al_2O_3 layer using the Cu/ Al_2O_3 /TiN CBRAM devices have not yet been reported.

On the other hand, one of the main challenges of CBRAM is to achieve high device uniformity and integration density. To have high-density memory, conventional three-dimensional (3D) FLASH has been conducted through-silicon-via (TSV) [27–30], which acts as interconnect in each stack. But one of the bottlenecks of TSV is high cost and large integration area. Joblot et al. [31] have reported the capability of Cu pillar for 3D interconnection technology. So, the conventional TSV technique of 3D FLASH can be also replaced by Cu pillar formation (i.e., stronger Cu filament in CBRAM structure) through 3D cross-point memory architecture for future below 11-nm technology node, which has been demonstrated previously [32]. In this case, each stack of cross-points memory could be connected through Cu pillar which would be a promising way for achieving ultra-high-density memory application. Therefore, the device size-dependent Cu pillar characteristics in the Cu/ Al_2O_3 /TiN structures have been also investigated for potential application.

In this study, impact of the device size and thickness on the Cu pillars and resistive switching memory characteristics using a single Al_2O_3 layer in the Cu/ Al_2O_3 /TiN CBRAM devices has been investigated. The amorphous Al_2O_3 film with a thickness of 18 nm and the device sizes are observed by transmission electron microscope

(TEM) image. By measuring 50 randomly picked devices, the empirical result tells that large size devices are promising for future Cu pillar applications. From cumulative probability of 50 devices, the Cu pillars can reach up to a high CC of 70 mA. Hence, the strong metallic path inside the Al_2O_3 layer can be used as a connecting way among the different stacks of high-density 3D memory devices. Long read endurance of 10^5 cycles of the large size devices at a high read voltage of –1.5 V ensures about the robustness of the Cu pillars or metallic paths. In addition, thickness-dependent resistive switching memory characteristics are also observed. Superior CBRAM characteristics such as high switching yield of 88%, lower average RESET current of approximately 328 μA , and acceptable resistance ratio of 9.6 are obtained for the 0.4- μm devices with a 2-nm-thick Al_2O_3 film under low voltage of ± 2 V, which is due to lower diffusion of Cu ions into the Al_2O_3 films under external bias. The resistive switching mechanism is based on the formation and dissolution of the Cu filaments into the Al_2O_3 films. Good data retention ability of >48 h is also obtained. This CBRAM device shows forming-free current-voltage (*I-V*) characteristics under a CC of 30 μA , even at lowest CC of 0.1 μA .

Methods

A silicon-dioxide (SiO_2) with a thickness of 200 nm was deposited on 8-in. Si wafer for device isolation. Then, a titanium-nitride (TiN) layer as a BE was deposited on SiO_2 /Si substrate. The thickness of TiN BE was approximately 200 nm. A SiO_2 film with a thickness of 150 nm was deposited for via-hole design. The via-holes with different sizes of 0.4×0.4 to $8 \times 8 \text{ }\mu\text{m}^2$ were patterned. To do the lift-off process, the pattern was coated by photo-resist (PR). Then, the via-hole and top electrode (TE) regions were opened. The Al_2O_3 layers with different thicknesses ranging from 2 to 20 nm were deposited by rf sputtering. The Al_2O_3 target with purity of 99.9% was used. During the deposition, argon (Ar) flow rate was 25 sccm. The deposition power and pressure were 80 W and 30 mTorr, respectively. The Cu as a TE was deposited by thermal evaporation. The thickness of Cu was approximately 40 nm. The deposition rate was 0.5 $\text{\AA}/\text{s}$. To avoid oxidation of Cu at elevated temperature, aluminum (Al) as a capping layer was deposited by using the same thermal evaporator. The thickness of Al was approximately 160 nm. Deposition rate was 1 $\text{\AA}/\text{s}$. Finally, lift-off process was performed to get the Al/Cu/ Al_2O_3 /TiN CBRAM devices. The memory device size and microstructure of an Al_2O_3 film was investigated by using TEM-JEOL 2100F system with energy of 200 keV and resolution of 0.2 nm. During electrical investigations of Cu pillar and resistive switching, the bias was applied on the Cu TE while the BE was grounded. The 20-nm-thick Al_2O_3 film was used to investigate the Cu pillars because the stronger Cu filament

will be formed under external positive bias on the TE. Other thicknesses of 2 to 10 nm were used to study the resistive switching characteristics. Fifty devices for each size and thickness of Al_2O_3 were measured randomly. All the electrical measurements were performed by Agilent 4156C precision semiconductor parameter analyzer (Agilent Technologies, Inc., Santa Clara, CA, USA).

Results and discussion

Figure 1a shows TEM image of an Al/Cu/ Al_2O_3 /TiN via-hole device. All layers are observed clearly. The device size of approximately $0.5 \times 0.5 \mu\text{m}^2$ is observed. Figure 1b shows high-resolution TEM image inside the via-hole region. The thickness of Al_2O_3 layer is approximately

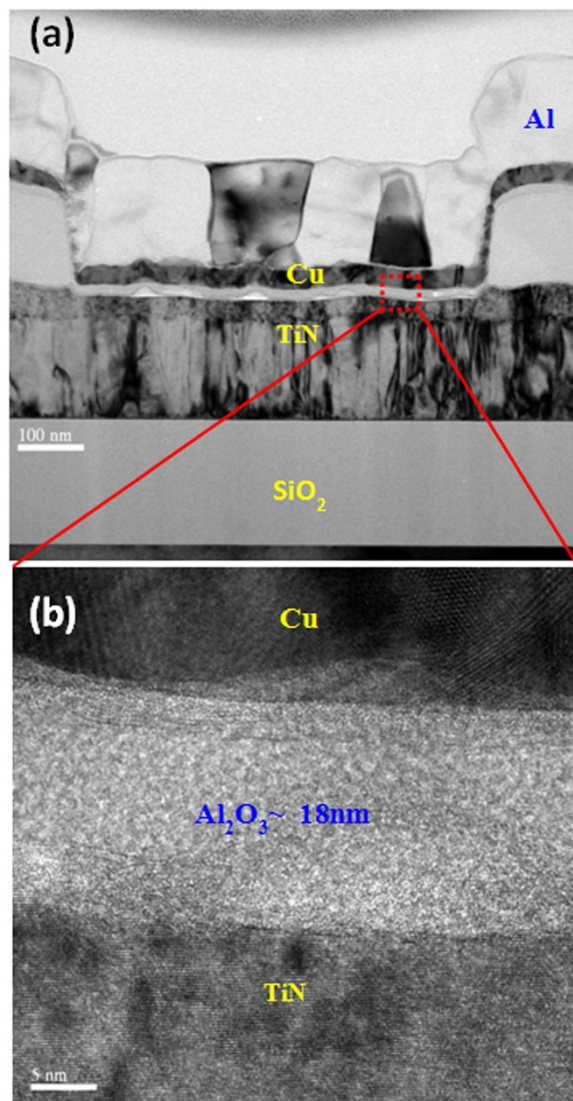


Figure 1 TEM images of an Al/Cu/ Al_2O_3 /TiN structure. (a) TEM image shows the device size of $0.5 \times 0.5 \mu\text{m}^2$. (b) HRTEM image shows Cu/ Al_2O_3 /TiN structure. The thickness of insulating layer is approximately 18 nm.

18 nm, including a thin TiO_xN_y layer on the TiN surface. This Al_2O_3 film shows amorphous. Due to the thicker Al_2O_3 film, the stronger Cu filament (or pillar) could be formed inside the via-hole region for 3D cross-point memory application, which has been discussed below.

The I - V characteristics of randomly measured 50 pristine devices with two different sizes viz. 8×8 and $0.4 \times 0.4 \mu\text{m}^2$ are shown in Figure 2. The thickness of Al_2O_3 film is 20 nm. The sweeping voltage direction is shown by the arrows 1 to 4, which also follows as $0 \rightarrow +5 \rightarrow 0 \rightarrow -1.1 \rightarrow 0$ and $0 \rightarrow +8 \rightarrow 0 \rightarrow -1 \rightarrow 0$ V for the devices with large and small sizes, respectively (Figure 2a,b). It is found that all 8- μm devices are operated at a high CC of 70 mA whereas many of the 0.4- μm devices show failure to reach even at a CC of 10 mA. By applying bias of -1 V on the TE, the 8- μm devices do not show RESET and few 0.4- μm devices show RESET. This

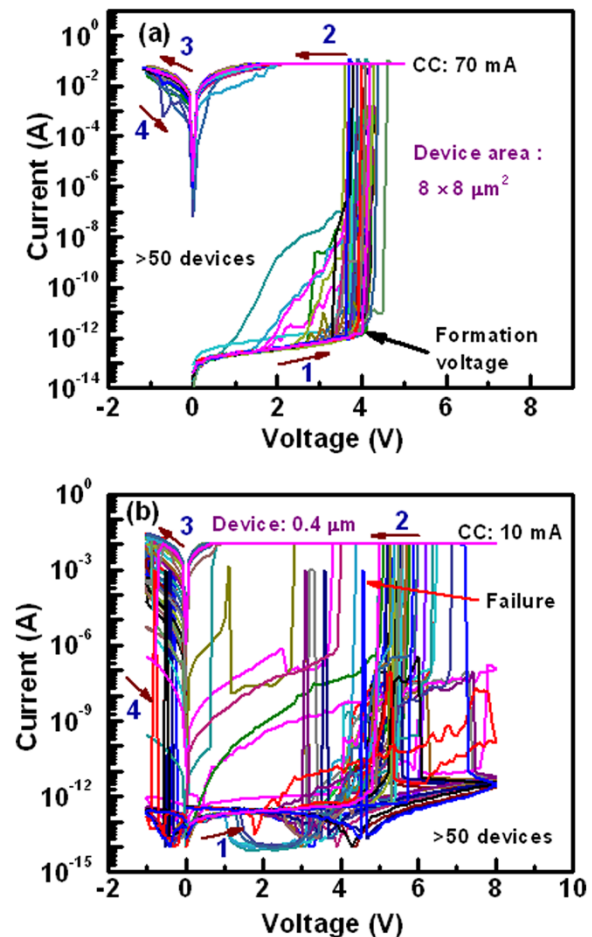


Figure 2 Current-voltage characteristics of the Cu pillars. I - V characteristics of arbitrarily measured 50 devices with device size of (a) $8 \times 8 \mu\text{m}^2$ under a high CC of 70 mA and of (b) $0.4 \times 0.4 \mu\text{m}^2$ under a CC of 10 mA. The smallest size devices have largest failure of the Cu pillars, due to the Joule heating. The thickness of the Al_2O_3 layer is 20 nm.

suggests that the Joule heating burns the small size devices at a high current as well as device size-dependent filament diameter. Heat dissipation of larger size devices is higher than the smaller size devices. Thermal conductivities of Cu, Al, Al_2O_3 , SiO_2 , TiN, and Si materials are 398, 244, 25.08, 1.38, 28.84, and 148 W/m/K, respectively [33]. This implies that heat will be dissipated through top electrode contact than the other sides. Therefore, the area of top electrode contact as well as device size will help to reduce heating effect, especially, when the device is operated at a high current of >10 mA. If the device does not show RESET, then stronger Cu filament (or pillar) is formed into the Al_2O_3 layer. The formation voltages (V_{form}) for the 8-, 4-, 2-, and 0.4- μm devices at 50% probability are 4.2, 4.5, 4.9, and 5.5 V, respectively (Figure 3a). Therefore, the value of V_{form} increases with decreasing the device sizes owing to lower leakage current as well as lower defects into the Al_2O_3

layer. On the other hand, the formation energy is lower for larger size devices than the smaller one owing to the higher diffusion rate of Cu ions with the area. The similar phenomena of Ag diffusion in SiO_2 layer by *in situ* TEM observation have been reported by Yang et al. [34]. The Cu diffusion in ZrO_2 layer by TEM observation was also reported by other group [35]. The number of successful devices with different device sizes ranging from 0.4×0.4 to $8 \times 8 \mu\text{m}^2$ is shown in Table 1. The device size of less than 2 μm can carry current of 10 mA, while the larger size of 4- μm device can carry high current of 70 mA. Most important thing is that the larger size devices show 100% success, while the failure is increased with decreasing device size. It is expected that stronger Cu pillar is needed for 3D integration of cross-point nonvolatile memory. This will be easy way and low cost for application of 3D cross-point memory [32]. Therefore, we need those devices which can sustain at high current for long time, and we find that, the devices with large area are compatible for this purpose. Figure 3b shows the statistical distribution of currents at low resistance state (LRS) for the device-to-devices. The mean value \bar{x} and the standard deviation (σ) of currents for the 4- μm devices at a read voltage (V_{read}) of 1 V are 49.96 and 9.33 mA, while those values for the 8- μm devices are 46.14 and 6.61 mA, respectively. The read current of the 8- μm devices is slightly lower than that of the 4- μm devices owing to lower formation voltage. This implies that small amount of Cu diffusion into the Al_2O_3 films for the larger size devices than the smaller sizes. However, uniformity of the high current carrying Cu pillars is better for the 8- μm devices than those of the 4- μm devices. The mechanism of Cu pillar formation inside the pristine device is as follows. These are basically the CBRAM devices; however, 20-nm-thick Al_2O_3 film is studied for demonstration, and further study for real application of the Cu pillars into the 1- μm -thick Al_2O_3 films is necessary. When the positive bias is applied on the active Cu electrode, the Cu^{z+} ($z = 1, 2$) ion is formed by oxidation, then those ions migrate through the switching medium in the presence of high electric field, and finally, they become reduced at the TiN BE. This formation process transforms the pristine device from its initial

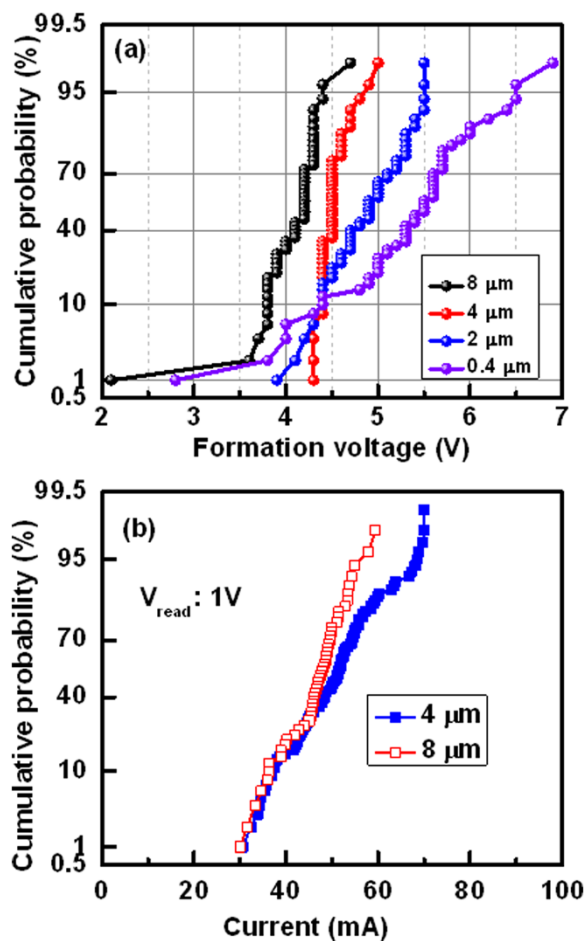


Figure 3 Statistical distribution of formation voltage and current of the Cu pillars. (a) Formation voltage increases with decreasing device area which suggests the higher Cu diffusion rate for large size devices. (b) Uniform current distribution at LRS of larger device sizes implies the probability of similar conduction path of the Cu pillars.

Table 1 Device size-dependent success and failure of the Cu pillars

Device size (μm^2)	Current compliance (mA)	Number of successful devices (%)
0.4×0.4	10	74
1×1	10	78
2×2	10	98
4×4	70	100
8×8	70	100

resistance state (IRS) to LRS as well as stronger Cu pillar is formed. By applying negative voltage on the TE, the Cu pillars of some smaller size devices are dissolved because of Joule heating. Robust Cu pillars have been investigated by measuring endurance properties below.

Figure 4 shows the read endurance characteristics with different negative read voltages. As it is bipolar device, the negative bias makes the RESET. After formation, we have increased the negative bias sequentially as -1 and -1.5 V on the TE. The current compliances are 10 and 70 μA for the 0.4- and 8- μm devices, respectively. For the 0.4- μm devices, a value of LRS is approximately 32 Ω (Figure 4a), while the value is approximately 20 Ω for the 8- μm devices (Figure 4b). This indicates that the

diameter of Cu pillar is larger for the 8- μm devices than the 0.4- μm devices, as shown schematic view in the inset. For the 0.4- μm devices, the LRS state is increased after approximately 40 and 30 k cycles for the read voltages of -1 and -1.5 V, respectively. The Cu pillar is broken easily after higher negative voltage on the TE, as shown schematically in the inset of Figure 4a. Robust read pulse endurance of $>10^5$ cycles are obtained for the 8- μm devices because of larger diameter of the Cu pillars, as shown schematically in the inset of Figure 4b. So, after formation of the conducting path, the possibility of deterioration of the paths is less which indicates the ability of Cu pillar for 3D cross-point architecture in the future. Beside the Cu pillar investigation, the resistive switching characteristics of the Cu/ Al_2O_3 /TiN CBRAM devices with smaller thickness (<10 nm) of Al_2O_3 layer are also important, which have been investigated below.

Figure 5 shows the typical I - V curves of the 8- μm devices with a 2-nm-thick Al_2O_3 film and a CC of 500 μA is applied. The sweeping voltage is shown by arrows 1 to 5. A low V_{form} of 1.65 V is observed for this thin Al_2O_3 film. Cumulative probability of 50 CBRAM devices with different size and thickness of the Al_2O_3 films is plotted (Figure 6a). The average values of V_{form} are 1.7, 2.4, and 3 V for the 8- μm devices while those values are 1.85, 2.7, and 3.4 V for the 0.4- μm devices with different thicknesses of Al_2O_3 film of 2, 5, and 10 nm, respectively. Those values of V_{form} are lower than the 20-nm-thick Al_2O_3 films (Figure 3a). For the 2-nm-thick Al_2O_3 films, tight distribution of V_{form} is found to be 1.6 to 1.75 V and 1.75 to 2.1 V for the 8- and 0.4- μm devices, respectively. Figure 6b shows cumulative probability of the leakage currents for the 8- and 0.4- μm devices with

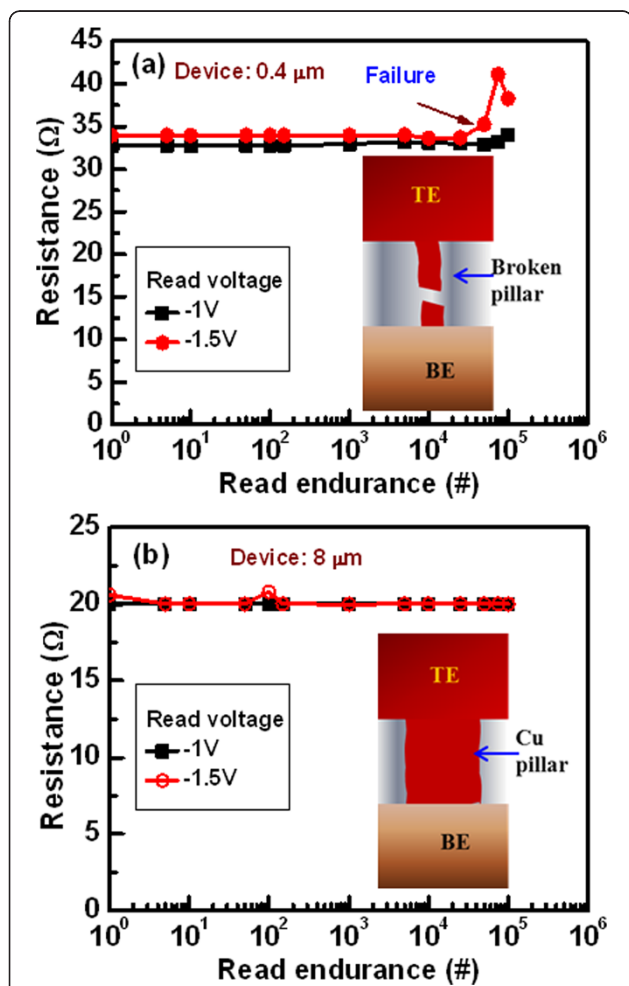


Figure 4 Read pulse endurance characteristics. (a) Read pulse endurance properties degraded at high negative voltage due to the Joule heating phenomena for the smallest size devices. The Cu pillar is broken during read endurance test, which is shown in schematic view. (b) For the large size devices, long endurance reveals the robustness of the Cu pillars inside the switching medium at a V_{read} of -1.5 V. Long read endurance of 10^5 cycles is obtained for the 8- μm devices. A stronger Cu pillar is formed into the Al_2O_3 films, which is shown in schematic view inside of figure.

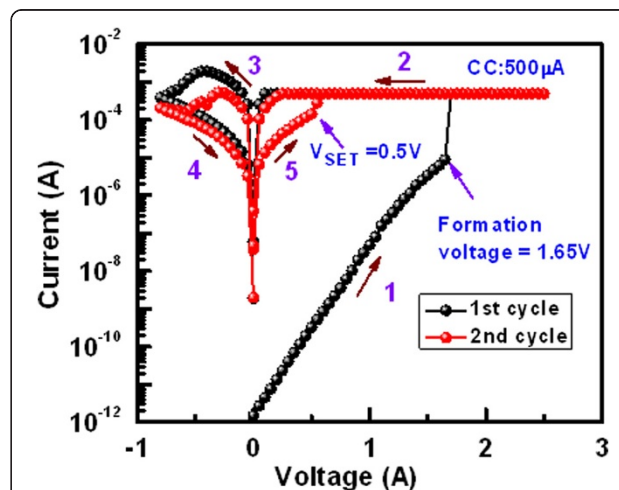
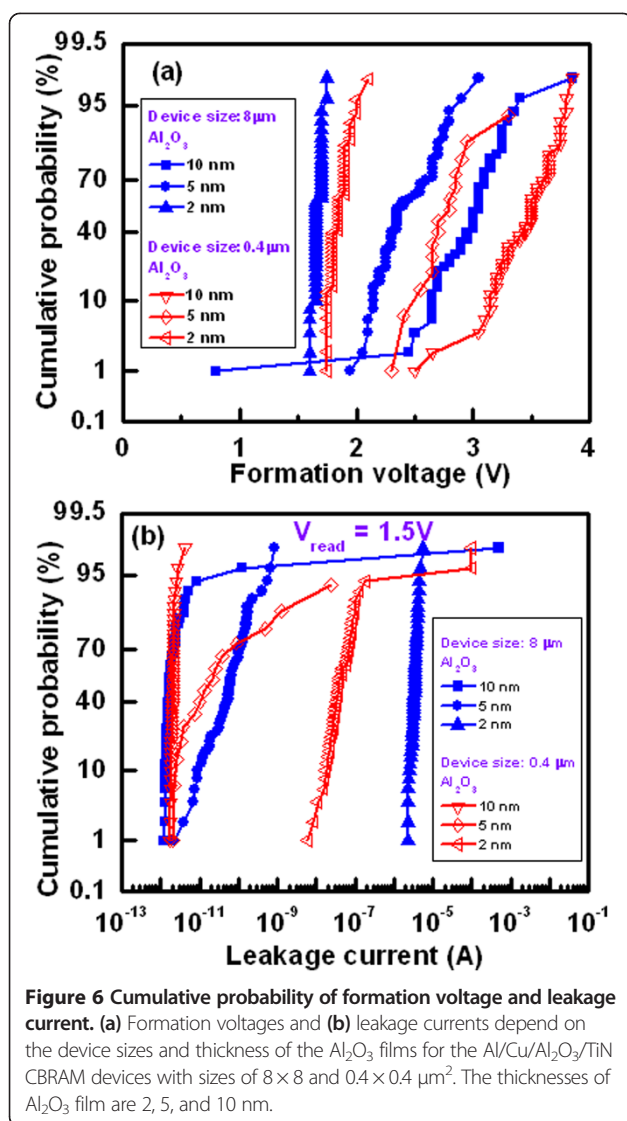


Figure 5 I - V switching characteristics. Typical current-voltage characteristics of the 8- μm devices with a 2-nm-thick Al_2O_3 film at a CC of 500 μA . A low formation voltage of 1.65 V is observed.



thicknesses of the Al_2O_3 films of 2, 5, and 10 nm. The leakage currents at 50% probability are found to be 3.4 μA , 60 pA, and 1.7 pA for the 8- μm devices while those values are found to be 39 nA, 22 pA, and 2.1 pA for the 0.4- μm devices with thicknesses of the Al_2O_3 films of 2, 5, and 10 nm, respectively. The 10-nm-thick Al_2O_3 films show device size-independent leakage currents, which is due to the limit of current measurement by our probe station. It is found that the variation of formation voltage is directly proportional to the switching material thickness and inversely proportional to the device size area. On the other hand, the leakage current shows the opposite nature of the formation voltage. It varies directly proportional to the device size and inversely proportional to the switching materials' thickness. It happens because the reduction in device size causes the decrement of defects inside the switching material which in turns increases its insulation

property. This causes the leakage current lower, and so, the required voltage to change its resistance state is more. The reduction in switching material thickness causes the higher possibility of electron tunneling through the insulator layer which causes the enhancement in leakage current. It is observed that the 2-nm-thick Al_2O_3 films show better uniformity of the formation voltages as well as the leakage currents. Both the RESET current (I_{RESET}) and voltage (V_{RESET}) at first cycle are found to be approximately 2 mA and -0.45 V, respectively (Figure 5). The SET voltages V_{SET} , V_{RESET} , and I_{RESET} at the second cycle are lower 0.5 V, -0.3 V, and approximately 540 μA than those of the values that are observed in the first cycle, respectively. The I_{RESET} is slightly higher than the current compliance because of thinner (2 nm) Al_2O_3 film. To dissolve more length of the Cu filaments or to increase high resistance state (HRS), higher negative voltage of -0.8 V is required. I - V curves imply that the RESET is happened through a slow deterioration process of the existing metallic filaments in its weak point by reduction due to the negative bias on the TE. A resistance ratio (HRS/LRS) at a V_{read} of 0.1 V is found to be 16, which is acceptable for application.

As we have mentioned, the switching mechanism is based on Cu filament formation/dissolution into the Al_2O_3 film under external bias, and this could be also understood indirectly by studying the breakdown phenomenon using two different top electrodes viz. Cu and Al, as shown in Figure 7. The thickness of the Al_2O_3 films is 5 nm. The average breakdown voltage (V_{BD}) of the randomly measured ten devices of the $\text{Al}/\text{Al}_2\text{O}_3/\text{TiN}$ structures is -4.99 V (i.e., -4.6 to -5.2 V) whereas this value of the $\text{Al}/\text{Cu}/\text{Al}_2\text{O}_3/\text{TiN}$ structures is 3.99 V (i.e., -3.7 to -4.3 V), as shown in Figure 7a. The value of V_{BD} is higher for the Al TE because the Al makes an additional oxide layer at the $\text{Al}/\text{Al}_2\text{O}_3$ interface. According to our previous report [36], the AlO_x layer was formed at the Al/TaO_x interface. It is also found that the value of V_{BD} for the $\text{Al}/\text{Cu}/\text{Al}_2\text{O}_3/\text{TiN}$ structures increases with increasing the thickness of Al_2O_3 layer, as shown in Figure 7b. If one can compare between the breakdown voltage and the formation voltage of the $\text{Al}/\text{Cu}/\text{Al}_2\text{O}_3/\text{TiN}$ structures with a 2-nm-thick Al_2O_3 layer, then the average value of breakdown voltage is higher than the formation voltage (-3.2 vs. 1.85 V). The similar trend is observed for all thicknesses of the Al_2O_3 films, as discussed above. This result reveals that the formation takes place due to the Cu ion migration through the Al_2O_3 layer. Under high electric field approximately 10^7 V/cm before breaking the stable Al-O bonds, electrochemically active Cu ions diffuse easily through the Al_2O_3 layer and make a metallic path under a low positive voltage applied on the TE. The Cu ion migration as well as filament formation into different switching layers under external bias was also reported by other groups [16-18,24].

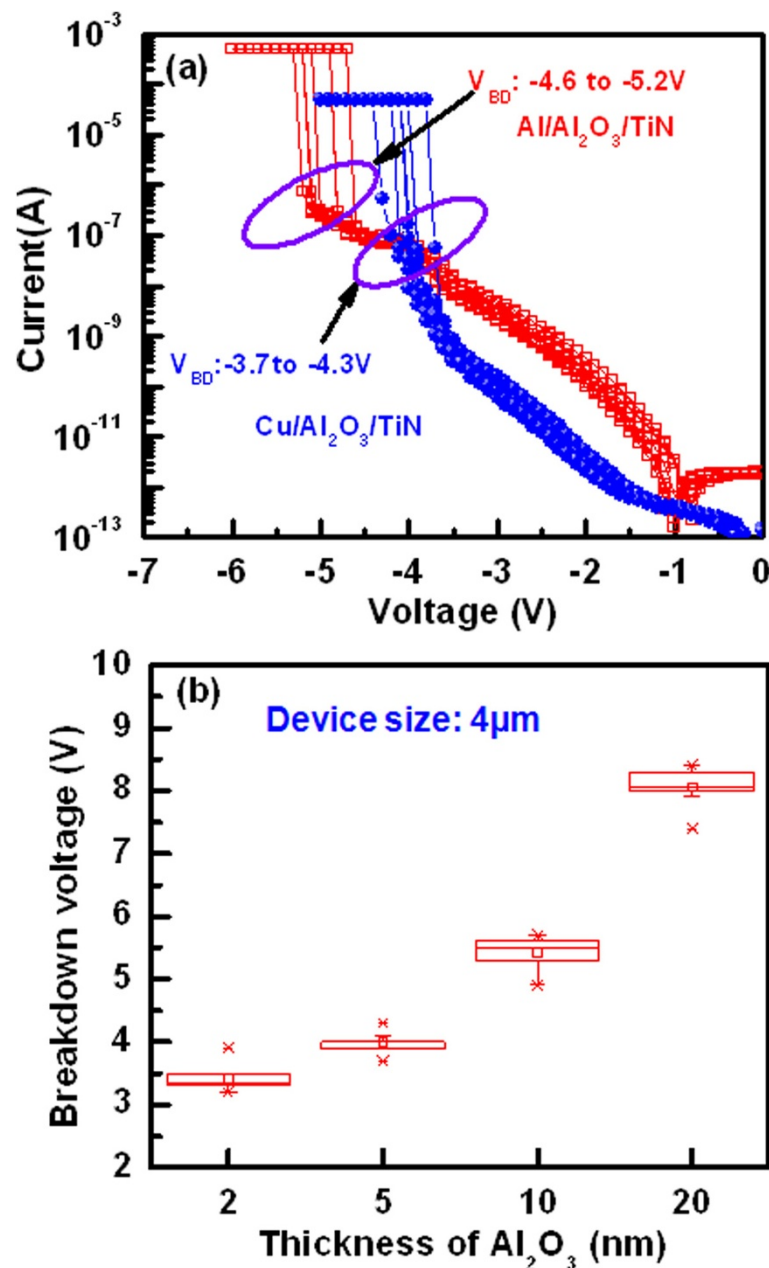
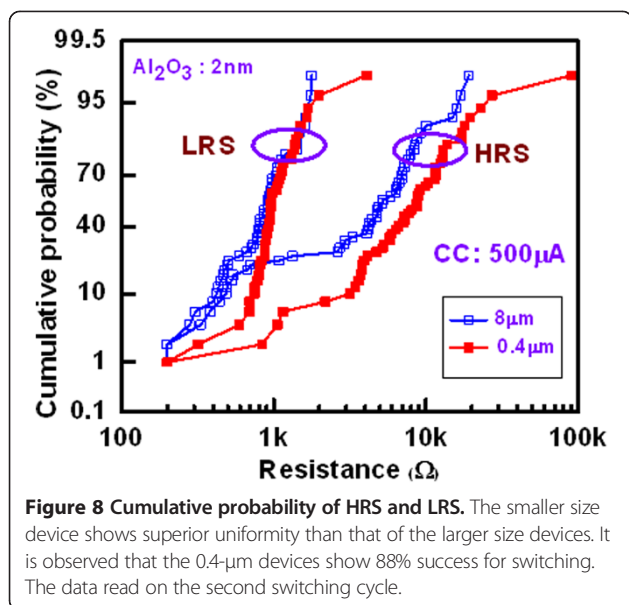


Figure 7 Thickness-dependent Al₂O₃ film breakdown phenomena with Cu and Al top electrodes. **(a)** *I-V* characteristics show the breakdown voltage of the Cu/Al₂O₃/TiN and Al/Al₂O₃/TiN structures. The higher breakdown voltage of Al/Al₂O₃/TiN than that of the Cu/Al₂O₃/TiN structure is owing to oxidized Al at the Al/Al₂O₃ interface during deposition by thermal evaporator. **(b)** The breakdown voltage of the Al/Cu/Al₂O₃/TiN structures increases with increasing the thickness of Al₂O₃ film.

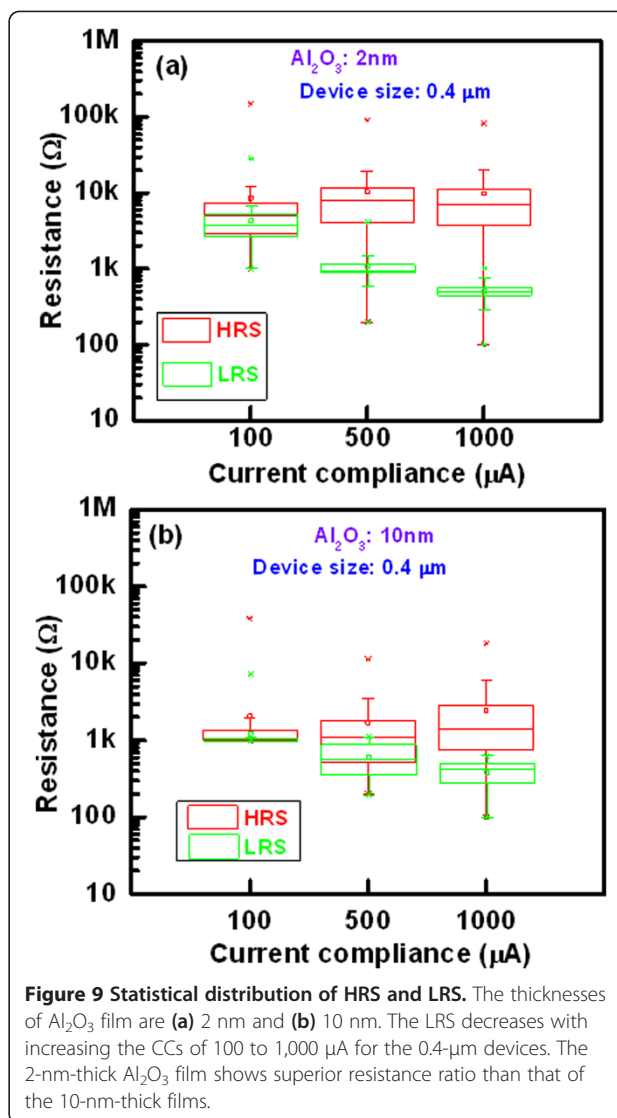
However, the switching uniformity is important of these CBRAM devices, which have been explained below.

Figure 8 shows cumulative probability of device-to-devices. The HRS and LRS for the 8- and 0.4-μm devices with a 2-nm-thick Al₂O₃ film are plotted. The average values of \bar{x}/σ at HRS and LRS are 5.34/4.44 kΩ and 895/407 Ω for the 8-μm devices, respectively, while those values are 10.3/12.9 kΩ and 1.07/539 kΩ for the 0.4-μm devices, respectively. The value of LRS is slightly lower for

the 8-μm devices than the 0.4-μm devices, which is owing to higher diffusion rate of Cu ion into the Al₂O₃ film under external bias. By considering the resistance ratio of >2, the 0.4-μm devices show higher switching yield than that of the 8-μm devices (88% vs. 74%). This suggests that the 0.4-μm devices have good switching uniformity. Figure 9 shows the statistical distribution of resistance states with different current compliances of 100, 500, and 1,000 μA for the 2- and 10-nm-thick Al₂O₃



films. Except few devices or without proper sweeping voltage/current, there is no memory window at a CC of 100 μA. However, the value of LRS decreases and HRS remains almost the same with increasing the CCs (Figure 9a,b). The resistance ratio increases with increasing the CCs. Table 2 represents the average values of LRS, HRS, and HRS/LRS for the 8- and 0.4-μm devices with different thicknesses of Al_2O_3 film of 2, 5, and 10 nm. To obtain the average values, 50 CBRAM devices were measured. It is obvious that the resistance ratio is higher at CC of 1 mA as compared to the value at a CC of 500 μA because of lower LRS value. At a CC of 500 μA, a high resistance ratio of 9.6 is obtained for the 0.4-μm devices with a 2-nm-thick Al_2O_3 film. In this case, more switchable devices are obtained (Figure 8), which is due to better control of Cu migration under external bias. The values of LRS are decreased with increasing both the device size and thickness of the Al_2O_3 films at a CC of 500 μA (Table 2), which can be explained by I_{RESET} later. Figure 10 shows cumulative probability of the RESET currents for the 8- and 0.4-μm devices with thicknesses of the Al_2O_3 films of 2, 5, and 10 nm at a CC of 500 μA. The average I_{RESET} values of the 2-, 5-, and 10-nm-thick Al_2O_3 films are found to be 706.1, 749.4, and 1,690 μA, respectively, for the 8-μm devices, while those values are found to be 327.5, 505.4, and 1,020 μA, respectively, for the 0.4-μm devices. It is observed that the I_{RESET} value decreases with decreasing the thickness of the Al_2O_3 films. Considering the thickness-dependent formation voltage (Figure 6a), the Cu ion can migrate more in the thicker Al_2O_3 films, resulting larger diameter of Cu filament. That is why the thicker Al_2O_3 film has higher RESET current. A lowest average RESET current of 327.5 μA with good uniformity is obtained for the 0.4-μm devices with a 2-nm-thick



Al_2O_3 film (Figure 10). As mentioned above, the formation voltage of the thinner Al_2O_3 films is lower than that of the thicker one. Under SET, small amount of Cu will be migrated for the thinner Al_2O_3 films as well as thinner diameter of the Cu filaments. That is why the LRS value of the thinner Al_2O_3 films is larger than the thicker one. Under RESET, the total length of the Cu filaments will be dissolved for the thinner Al_2O_3 films because of both higher electric field and thinner filament diameter than that of the thicker one. On the other hand, interface-type switching or even no RESET is observed for the thicker Al_2O_3 films. Therefore, HRS value of the thinner Al_2O_3 films is higher than those of the thicker one. It can be concluded that thicker Al_2O_3 film can be used for the Cu pillars to apply in 3D cross-point memory and thinner one can be used for the nonvolatile resistive switching memory, and data retention test is shown below.

Table 2 Device size- and thickness-dependent LRS, HRS, and resistance ratio with different current compliances

Thickness of Al ₂ O ₃ (nm)	Device size (μm ²)	Average value (Ω) and resistance ratio of HRS/LRS					
		CC: 500 μA			CC: 1 mA		
		LRS	HRS (k)	HRS/LRS	LRS	HRS (k)	HRS/LRS
2	0.4×0.4	1070	10.3	9.63	502	9.8	19.55
	8×8	895	5.34	5.97	384	22.3	58.10
5	0.4×0.4	826	4.64	5.62	487	3.6	7.39
	8×8	652	4.54	6.96	364	18.3	50.27
10	0.4×0.4	572	1.71	3.00	394	2.48	6.3
	8×8	492	1.48	3.00	343	2.05	6.0

Figure 11 shows data retention characteristics for the 0.4-μm devices with a 2-nm-thick Al₂O₃ film. It is found the stable retention characteristics of >48 h at a CC of 1 mA (Figure 11a). The LRS is increased (slightly) with retention time, however, long time retention of 48 h at a CC of 300 μA is obtained (Figure 11b), which may be the higher dissolution rate of the existing filament at lower CC. The resistance ratio for a CC of 300 μA is higher than the ratio at CC of 1 mA (100 vs. 10). At a lower CC, the small amount of the Cu atoms is responsible for the conducting filament formation. If small amount of Cu atoms from the thinner filament may be dissolved by neighbor defects into the AlO_x film or dissolved by reading data, then both HRS and LRS could be increased with time. For larger diameter of the Cu filaments under higher CC, it shows stable with time because dissolution of small amount Cu from the filaments does not affect the filament resistance of LRS, or even HRS. However, further study is needed to form a stronger Cu filament with thinner diameter. By adjusting measurement parameters, this CBRAM device shows forming-free *I-V* characteristics

under a low CC of 30 μA and a RESET current of <30 μA with a high resistance ratio of >10⁵ at a read voltage of +0.2 V (Figure 12a). This device is operated even at a lowest CC of 0.1 μA (Figure 12b) with a large resistance ratio of >10⁴, which is very useful for future nanoscale nonvolatile memory applications.

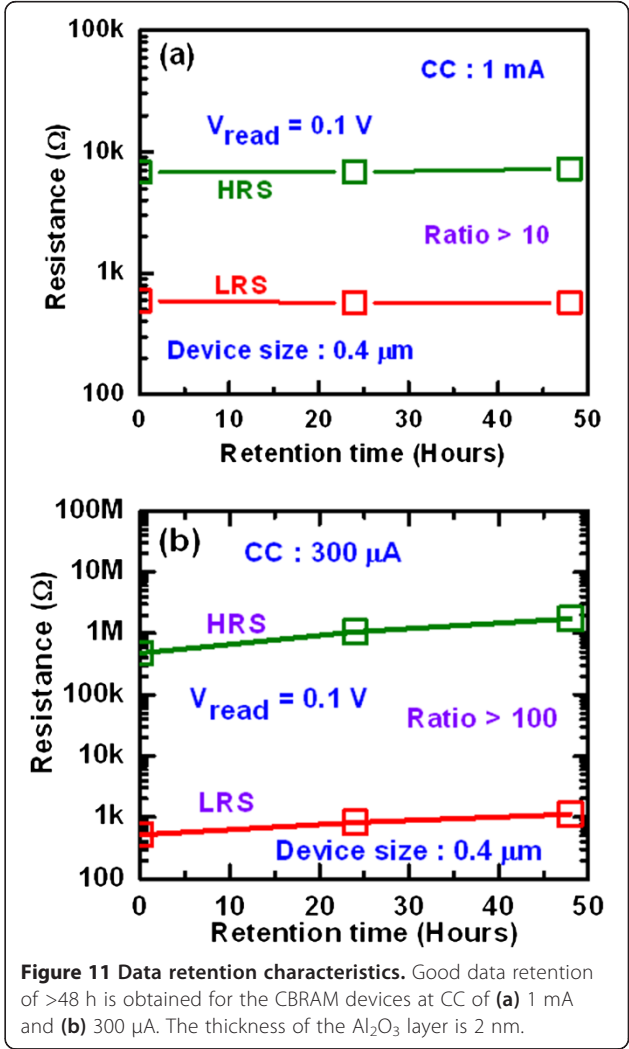
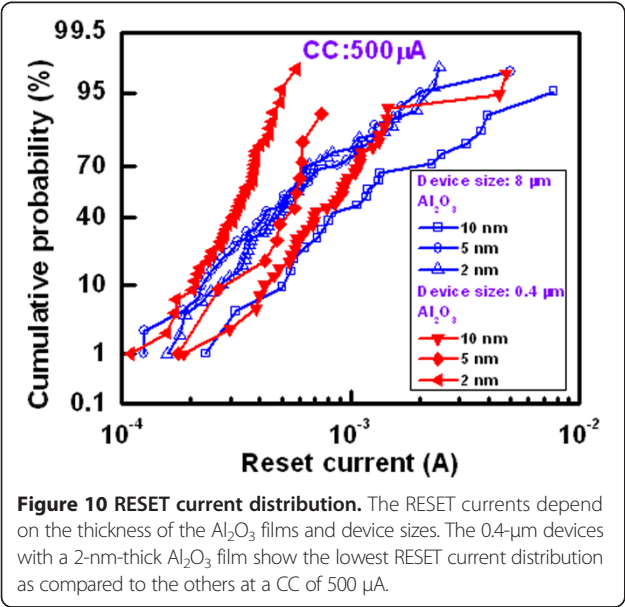


Figure 10 RESET current distribution. The RESET currents depend on the thickness of the Al₂O₃ films and device sizes. The 0.4-μm devices with a 2-nm-thick Al₂O₃ film show the lowest RESET current distribution as compared to the others at a CC of 500 μA.

Figure 11 Data retention characteristics. Good data retention of >48 h is obtained for the CBRAM devices at CC of (a) 1 mA and (b) 300 μA. The thickness of the Al₂O₃ layer is 2 nm.

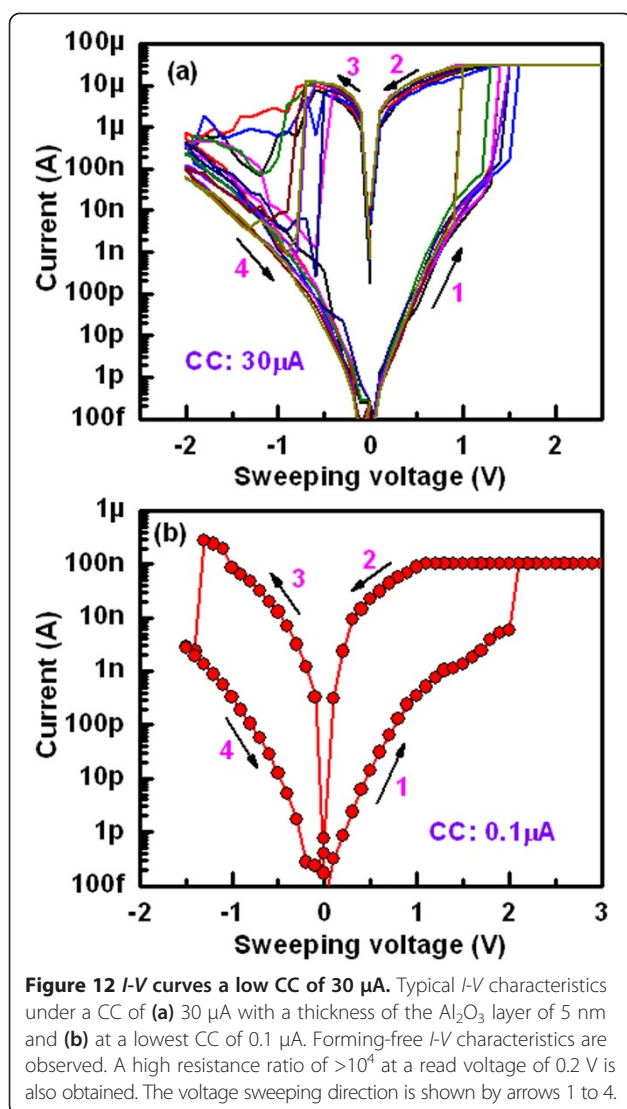


Figure 12 *I-V* curves a low CC of 30 μA . Typical *I-V* characteristics under a CC of (a) 30 μA with a thickness of the Al_2O_3 layer of 5 nm and (b) at a lowest CC of 0.1 μA . Forming-free *I-V* characteristics are observed. A high resistance ratio of $>10^4$ at a read voltage of 0.2 V is also obtained. The voltage sweeping direction is shown by arrows 1 to 4.

Conclusions

The device size- and thickness-dependent Cu pillars and resistive switching memory characteristics using the Al/Cu/ Al_2O_3 /TiN CBRAM devices have been investigated. The stronger Cu pillars with yield of 100% are formed into the Al_2O_3 films for the larger size devices at a high CC of 70 mA, which is due to the easy heat dissipation effect. Robust Cu pillar with a long endurance of $>10^5$ cycles is obtained even a high negative voltage of -1.5 V, which promises for future 3D cross-point memory applications. Improved resistive switching memory characteristics such as high switching yield of 88%, low voltage operation of ± 2 V, and lower average RESET current of 327.5 μA for a CC of 500 μA are obtained for the 0.4- μm devices with a 2-nm-thick Al_2O_3 film. The formation/dissolution of the Cu filaments into a 2-nm-thick Al_2O_3 film is responsible to have better switching characteristics under external bias because of thinner film. On the other

hand, Cu diffusion rate is higher for the larger size and thicker film which will have inferior switching characteristics, however, give us superior Cu pillars. Good data retention characteristics of 48 h are obtained at a CC of 300 μA . This device shows forming-free *I-V* characteristics under a lowest CC of 0.1 μA with a high resistance ratio of $>10^4$. This strategy on the Cu pillars and resistive switching memory characteristics of the Cu/ Al_2O_3 /TiN CBRAM devices will help to develop in future 3D cross-point architecture with low cost applications.

Competing interests

The authors declare that they have no competing interests.

Authors' contributions

RP fabricated the CBRAM devices under the instruction of SM. DJ helped also partially to fabricate the devices. RP measured all the devices under the instruction of SM. SR and DJ measured also the CBRAM devices partially under the instruction of SM. All authors contributed to the revision of the manuscript, and they approved it for publication.

Acknowledgements

This work was supported by National Science Council (NSC) Taiwan, under contract no. NSC-102-2221-E-182-057-MY2. The authors are also grateful to Electronics and Optoelectronics Research Laboratories (EOL)/Industrial Technology Research Institute (ITRI) in Hsinchu, Taiwan for their experimental support.

Received: 29 November 2014 Accepted: 8 December 2014

Published: 23 December 2014

References

- Prakash A, Jana D, Maikap S: TaO_x based resistive switching memories: prospective and challenges. *Nanoscale Res Lett* 2013, **8**:418.
- Yang JJ, Strukov DB, Stewart DR: Memristive devices for computing. *Nat Nanotechnology* 2013, **8**:13.
- Torrezan AC, Strachan JP, Medeiros-Ribeiro G, Williams RS: Sub-nanosecond switching of a tantalum oxide memristor. *Nanotechnology* 2011, **22**:485203.
- Lee HY, Chen PS, Wu TY, Chen YS, Wang CC, Tzeng PJ, Lin CH, Chen F, Lien CH, Tsai MJ: Low power and high speed bipolar switching with a thin reactive Ti buffer layer in robust HfO_2 based RRAM. *Tech Dig - Int Electron Devices Meet.* San Francisco, CA; 2008:1–4.
- Chen YS, Lee HY, Chen PS, Liu WH, Wang SM, Gu PY, Hsu YY, Tsai CH, Chen WS, Chen F, Tsai MJ, Lien C: Robust high-resistance state and improved endurance of HfO_2 resistive memory by suppression of current overshoot. *IEEE Electron Device Lett* 2011, **32**:1585.
- Wu Y, Yu S, Lee B, Wong HSP: Low-power TiN/ Al_2O_3 /Pt resistive switching device with sub-20 μA switching current and gradual resistance modulation. *J Appl Phys* 2011, **110**:094104.
- Lin CY, Wu CY, Hu C, Tseng TY: Bistable resistive switching in Al_2O_3 memory thin films. *J Electrochem Soc* 2007, **154**:G189.
- Banerjee W, Maikap S, Rahaman SZ, Prakash A, Tien TC, Li WC, Yang JR: Improved resistive switching memory characteristics using core-shell IrO_x nano-dots in $\text{Al}_2\text{O}_3/\text{WO}_x$ bilayer structure. *J Electrochem Soc* 2012, **159**:H177.
- Prakash A, Maikap S, Banerjee W, Jana D, Lai CS: Impact of electrically formed interfacial layer and improved memory characteristics of $\text{IrO}_x/\text{high-}\kappa/\text{W}$ structures containing AlO_x , GdO_x , HfO_x , and TaO_x switching materials. *Nanoscale Res Lett* 2013, **8**:379.
- Afanas'ev VV, Stesmans A: Internal photoemission at interfaces of high- κ insulators with semiconductors and metals. *J Appl Phys* 2007, **102**:08130.
- Yu HY, Li MF, Cho BJ, Yeo CC, Joo MS, Kwong DL, Pan JS, Ang CH, Zheng JZ, Ramanathan S: Energy gap and band alignment for $(\text{HfO}_2)_x(\text{Al}_2\text{O}_3)_{1-x}$ on (100) Si. *Appl Phys Lett* 2002, **81**:376.
- Robertson J: High dielectric constant oxides. *Eur Phys J Appl Phys* 2004, **28**:265.
- Dean JA: Lange's Handbook of Chemistry. 896.

14. Wu Y, Lee B, Philip Wong HSP: **Ultra-low power Al_2O_3 -based RRAM with 1 μA reset current.** In *International Symposium on VLSI Technology Systems and Applications (VLSI-TSA)*. Hsinchu; 2010:136–137.
15. Kund M, Beitel G, Pinnow CU, Röhr T, Schumann J, Symanczyk R, Ufert KD, Müller G: **Conductive bridging RAM (CBRAM): An emerging non-volatile memory technology scalable to sub 20 nm.** In *Tech Dig - Int Electron Devices Meet. (IEDM)*. Washington, DC: 2005:754–757.
16. Rahaman SZ, Maikap S, Das A, Prakash A, Wu YH, Lai CS, Tien TC, Chen WS, Lee HY, Chen FT, Tsai MJ, Chang LB: **Enhanced nanoscale resistive switching memory characteristics and switching mechanism using high-Ge-content $\text{Ge}_{0.5}\text{Se}_{0.5}$ solid electrolyte.** *Nanoscale Research Lett* 2012, **7**:614.
17. Valov I, Waser R, Jameson JR, Kozicki MN: **Electrochemical metallization memories-fundamentals, applications, prospects.** *Nanotechnology* 2011, **22**:254003.
18. Jameson JR, Gilbert N, Koushan F, Saenz J, Wang J, Hollmer S, Kozicki M, Derhacopian N: **Quantized conductance in $\text{Ag}/\text{GeS}_2/\text{W}$ conductive-bridge memory cells.** *IEEE Electron Device Lett* 2012, **33**:257.
19. Kwak JS, Chi EJ, Choi JD, Park SW, Baik HK, So MG, Lee SM: **Prediction of solid-state amorphizing reaction using effective driving force.** *J Appl Phys* 1995, **78**:983.
20. Banno N, Sakamoto T, Iguchi N, Sunamura H, Terabe K, Hasegawa T, Aono M: **Diffusivity of Cu ions in solid electrolyte and its effect on the performance of nanometer-scale switch.** *IEEE Trans Electron Devices* 2008, **55**:3283.
21. Kaeriyama S, Sakamoto T, Sunamura H, Mizuno M, Kawaura H, Hasegawa T, Terabe K, Nakayama T, Aono M: **A nonvolatile programmable solid-electrolyte nanometer switch.** *IEEE J Solid-State Circuits* 2005, **40**:168.
22. Xu Z, Bando Y, Wang W, Bai X, Golberg D: **Real-time *in-situ* HRTEM-resolved resistance switching of Ag_2S nanoscale ionic conductor.** *ACS Nano* 2010, **4**:2515.
23. Terabe K, Hasegawa T, Nakayama T, Aono M: **Quantized conductance atomic switch.** *Nature* 2005, **433**:47.
24. Goux L, Opsomer K, Degraeve R, Müller R, Detavernier C, Wouters DJ, Jurczak M, Altimime L, Kittl JA: **Influence of the Cu-Te composition and microstructure on the resistive switching of Cu-Te/ Al_2O_3 /Si cells.** *Appl Phys Lett* 2011, **99**:053502.
25. Sleiman A, Sayers PW, Mabrook MF: **Mechanism of resistive switching in Cu/ AlO_x /W nonvolatile memory structures.** *J Appl Phys* 2013, **113**:164506.
26. Belmonte A, Kim W, Chan BT, Heylen N, Fantini A, Houssa M, Jurczak M, Goux L: **90 nm W/ Al_2O_3 /TiW/Cu 1T1R CBRAM cell showing low-power, fast and disturb-free operation.** *International Memory Workshop (IMW)* 2013.
27. Tanaka H, Kido M, Yahashi K, Oomura M, Katsumata R, Kito M, Fukuzumi Y, Sato M, Nagata Y, Matsuo Y: **Bit cost scalable technology with punch and plug process for ultra high density flash memory.** Kyoto: Tech Dig Symp VLSI Technol; 2007:14–15.
28. Kim W, Choi S, Sung J, Lee T, Park C, Ko H, Jung J, Yoo I, Park Y: **Multi-layered vertical gate NAND flash overcoming stacking limit for terabit density storage.** Honolulu, HI: Tech Dig Symp VLSI Technol; 2009:188–189.
29. Jang J, Kim HS, Cho W, Cho H, Kim J, Shim S, Jang Y, Jeong J, Son BK, Kim DW, Kim K, Shim JJ, Lim JS, Kim KH, Yi SY, Lim JY, Chung D, Moon HC, Hwang S, Lee JW, Son YH, Chung UI, Lee WS: **Vertical cell array using TCAT (Terabit Cell Array Transistor) technology for ultra high density NAND flash memory.** Honolulu, HI: Tech Dig Symp VLSI Technol; 2009:192–193.
30. Katsumata R, Kito M, Fukuzumi Y, Kido M, Tanaka H, Komori Y, Ishiduki M, Matsunami J, Fujiwara T, Nagata Y, Zhang L, Iwata Y, Kirisawa R, Aochi H, Nitayama A: **Pipe-shaped BiCS flash memory with 16 stacked layers and multi-level-cell operation for ultra high density storage devices.** Honolulu, HI: Tech Dig Symp VLSI Technol; 2009:136–137.
31. Joblot S, Bar P, Sibuet H, Ferrandon C, Reig B, Jan S, Arnaud C, Lamy Y, Coudrain P, Coffy R, Boillon O, Carpentier JF: **Copper pillar interconnect capability for mm wave applications in 3D integration technology.** *Microelectron Eng* 2013, **107**:72.
32. Maikap S, Panja R, Jana D: **Copper pillar and memory characteristics using Al_2O_3 switching material for 3D architecture.** *Nanoscale Res Lett* 2014, **9**:366.
33. **A MEMS clearinghouse and information portal for the MEMS and nanotechnology community.** <http://www.memsnet.org/news/> and <http://en.wikipedia.org/wiki/Silicon>.
34. Yang Y, Gao P, Gaba S, Chang T, Pan X, Lu W: **Observation of conducting filament growth in nanoscale resistive memories.** *Nature Comm* 2012, **3**:1.
35. Liu Q, Sun J, Lv H, Long S, Yin K, Wan N, Li Y, Sun L, Liu M: **Real-Time observation on dynamic growth/dissolution of conductive filaments in oxide-electrolyte-based ReRAM.** *Adv Mater* 2012, **24**:1844.
36. Prakash A, Maikap S, Chen WS, Lee HY, Chen F, Tien TC, Lai CS: **Device size-dependent improved resistive switching memory performance.** *IEEE Trans Nanotech* 2014, **13**:409.

doi:10.1186/1556-276X-9-692

Cite this article as: Panja et al.: Impact of device size and thickness of Al_2O_3 film on the Cu pillar and resistive switching characteristics for 3D cross-point memory application. *Nanoscale Research Letters* 2014 **9**:692.

Submit your manuscript to a SpringerOpen[®] journal and benefit from:

- Convenient online submission
- Rigorous peer review
- Immediate publication on acceptance
- Open access: articles freely available online
- High visibility within the field
- Retaining the copyright to your article

Submit your next manuscript at ► springeropen.com